

Electronic Supplementary Information

New approach for preparation of phenylbutazone polymorphs

Mukhammet N. Gabdulkhaev,^a Anastasia V. Simdyanova,^a Dmitrii N. Bolmatenkov,^a Aidar T. Gubaidullin,^{a,b} Timur A. Mukhametzyanov,^a Marat A. Ziganshin,^a Valery V. Gorbatchuk^{*a}

^a A.M. Butlerov Institute of Chemistry, Kazan Federal University, Kremlevskaya 18, 420008 Kazan, Russian Federation. E-mail: Valery.Gorbatchuk@kpfu.ru

^b A.E. Arbuzov Institute of Organic and Physical Chemistry, Akad. Arbuzova, 8, 420088 Kazan, Russia

Content:

Fig. S1 Image of crystalline PBZ (phenylbutazone) solvate with acetonitrile	2
Fig. S2 Optical microscopy images of PBZ solvates with hydrocarbons and polychloromethanes	2
Fig. S3 Optical microscopy images of PBZ polymorphs and guest-free forms	3
Fig. S4 Comparison of powder X-ray diffraction patterns of β and β' forms	4
Fig. S5 Comparison of powder X-ray diffraction patterns of β polymorph prepared from PBZ melt under different conditions	5
Fig. S6 TG/DSC and PXRD data for β polymorph prepared by different methods	6
Fig. S7 Thermomicroscopy images of β polymorph prepared from PBZ solution in ethanol	6
Fig. S8 Comparison of powder X-ray diffraction pattern of $\delta+\beta'$ form and sum of diffractograms of δ and β' forms	7
Fig. S9 Comparison of powder X-ray diffractograms of δ and δ' forms	8
Table S1 Powder X-ray diffraction peaks of phenylbutazone polymorphs and solvates	9
Fig. S10 Indexing results for diffraction pattern of δ' form	10
Figs S11 Images of the 4-OH-PBZ (4-hydroxyphenylbutazone) crystals	11
Table S2 Torsion angles of phenylbutazone in crystals of PBZ·MeCN solvate and 4-OH-PBZ	11
Fig. S12 Powder X-ray diffractograms of 4-OH-PBZ: experimental and simulated from SCXRD data	12
Fig. S13 Powder X-ray diffractograms of α polymorph of phenylbutazone	13
Fig. S14 Powder X-ray diffraction patterns of PBZ·0.20CCl ₄ solvate and the product of its saturation with n-hexane vapor	13
Fig. S15 TG/DSC/MS data for the product of PBZ·0.20CCl ₄ saturation with n-hexane vapor	14
Fig. S16 TG/DSC/MS data for δ form prepared by guest repulsion from PBZ·0.44c-C ₆ H ₁₂ with EtOH vapor	14
Fig. S17 Comparison of PXRD pattern of commercial δ form with that of prepared by guest repulsion from PBZ·0.44c-C ₆ H ₁₂ with EtOH vapor	15
Fig. S18 Indexing results for XRPD diffractogram of β' polymorph	16
Fig. S19 Indexing results for XRPD diffractogram of δ polymorph prepared by guest repulsion from PBZ·0.44c-C ₆ H ₁₂ with EtOH vapor	17
Table S3 Lists of PXRD peaks for PBZ polymorphs, guest-free forms and solvates	18



Fig. S1 Image of the crystalline PBZ solvate with acetonitrile

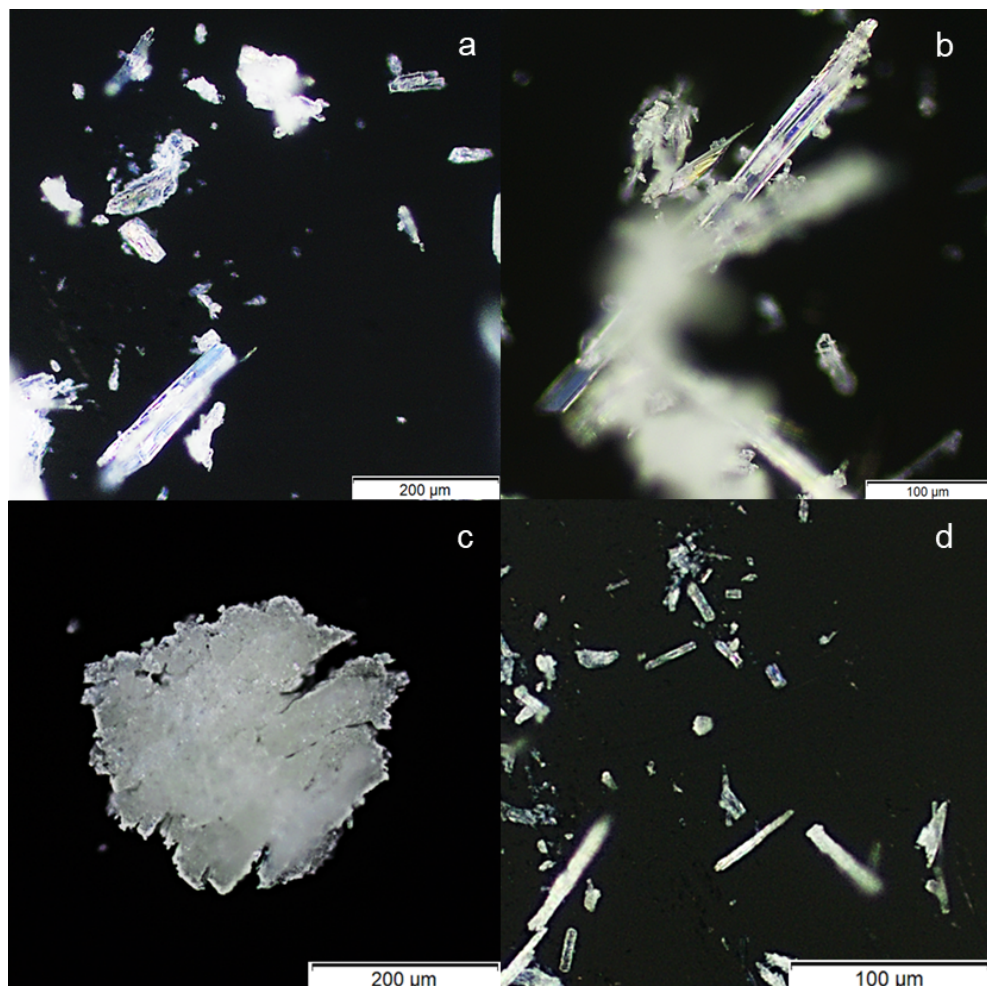


Fig. S2 Optical microscopy images of the PBZ solvates with hydrocarbons and polychloromethanes in polarized reflected light: (a) benzene, (b) tetrachloromethane, (c) chloroform, (d) cyclohexane.

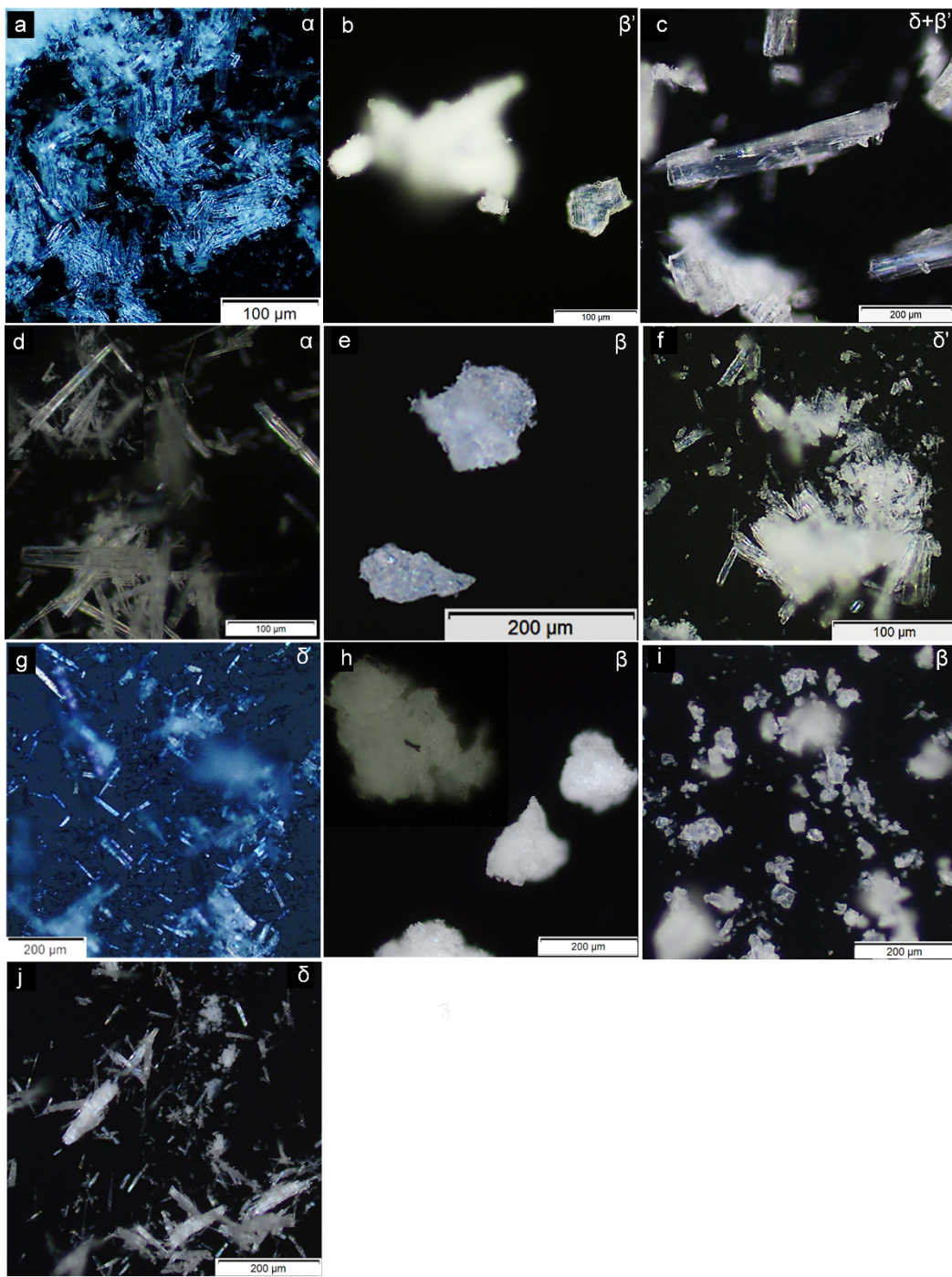


Fig. S3 Optical microscopy images of PBZ polymorphs and guest-free forms in polarized reflected light: (a) α polymorph prepared in ternary ‘PBZ·0.44*c*-hexane +*n*-hexane (vap)’ system; (b) β' polymorph prepared in binary PBZ+MeCN system at RT; (c) $\delta+\beta'$ form prepared by drying PBZ·MeCN solvate in air at RT; (d) α polymorph obtained by dissolution of PBZ·0.20CCl₄ solvate in ethanol and subsequent drying; (e) β polymorph prepared by cooling PBZ melt in air and grinding; (f) δ' polymorph prepared by heating the $\delta+\beta'$ mixture to 92 °C and then cooling to RT in air; (g) δ polymorph (commercial form); (h) β polymorph prepared by crystallization of PBZ from solution in ethanol at RT; (i) β polymorph prepared by cooling PBZ melt in argon flow and grinding; (j) δ polymorph prepared in ternary ‘PBZ·0.44*c*-hexane +EtOH (vap)’ system.

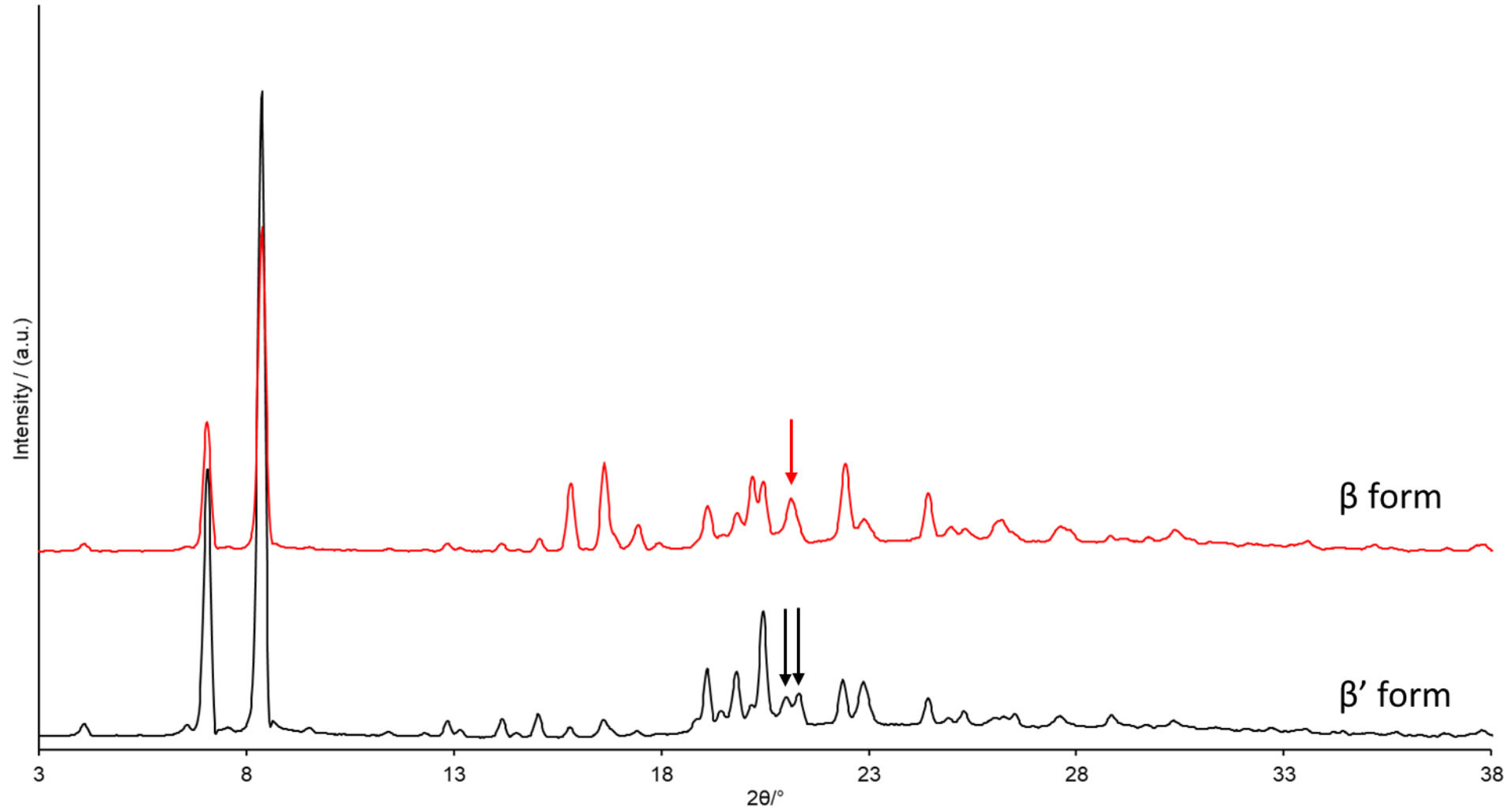
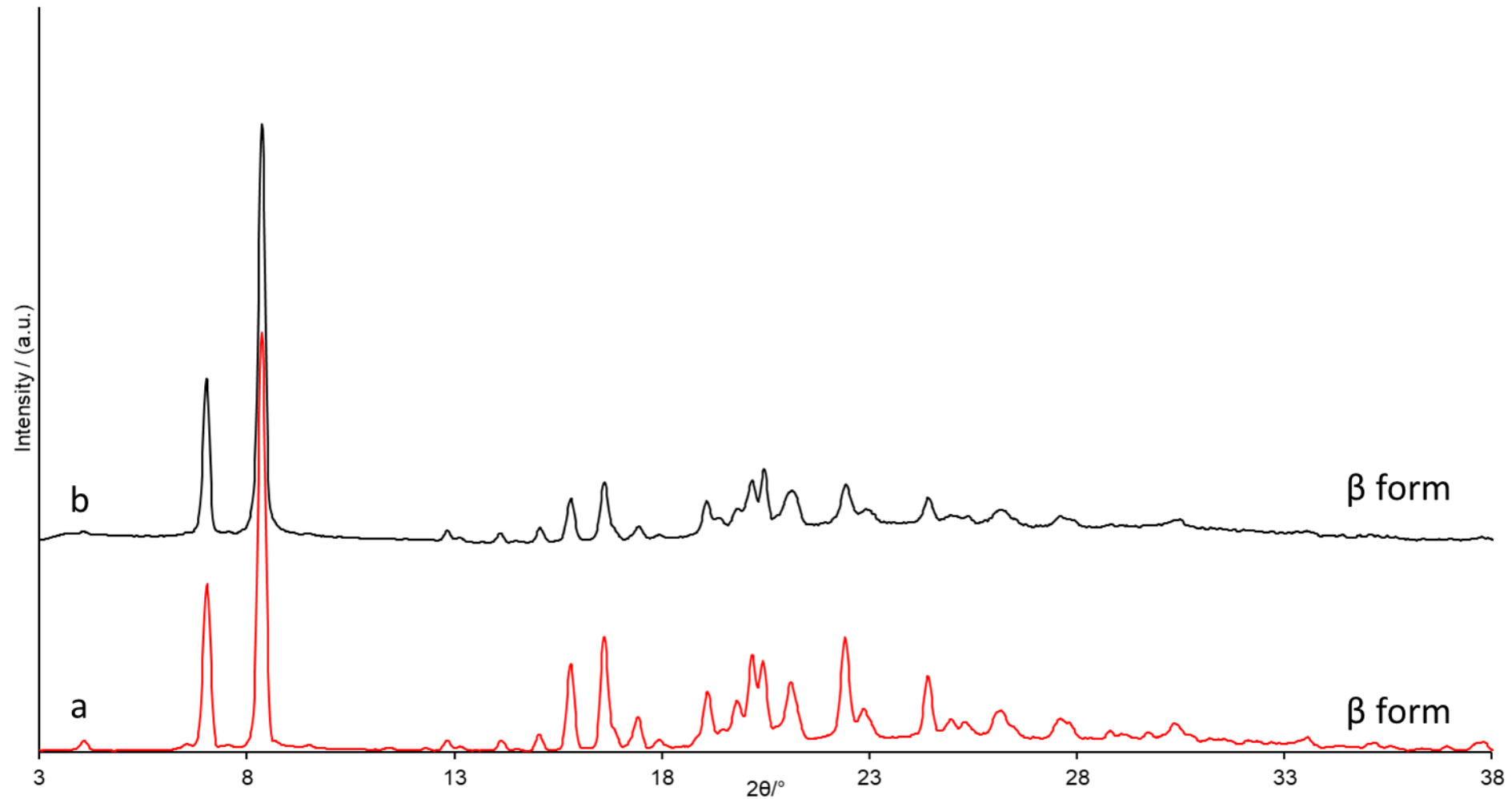


Fig. S4 Comparison of powder X-ray diffractograms of β polymorph prepared by cooling PBZ melt in argon flow and grinding and β' form. Diffractograms are corrected using standard silicon powder SRM 640d, and background was subtracted. Arrows indicate peaks with significant difference in position.



. S5 Comparison of powder X-ray diffractograms of β polymorph prepared by (a) by cooling PBZ melt in air and grinding, (b) by cooling PBZ melt in argon flow and grinding. Diffractograms are corrected using standard silicon powder SRM 640d, and background was subtracted.

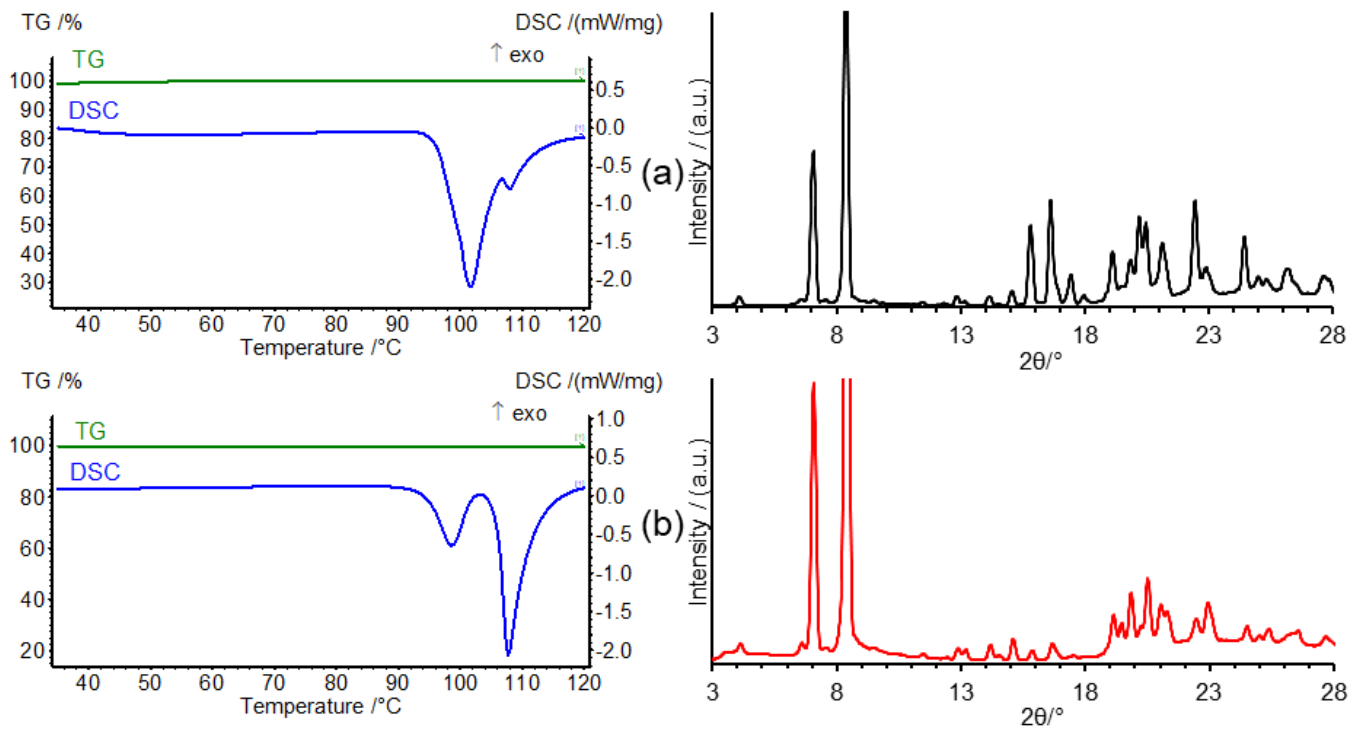


Fig. S6 TG/DSC and powder X-ray diffractometry data for β polymorph (a) prepared by cooling PBZ melt in air at RT (onset point and enthalpy are 96 $^{\circ}\text{C}$ and 21.6 kJ mol^{-1} for the first transition and 106 $^{\circ}\text{C}$ and 4 kJ mol^{-1} for the second transition, respectively), (b) prepared by crystallization of from PBZ solution in ethanol at RT (onset point and enthalpy are 95 $^{\circ}\text{C}$ and 6.6 kJ/mol for the first transition and 105 $^{\circ}\text{C}$ and 17 kJ mol^{-1} for the second transition, respectively).

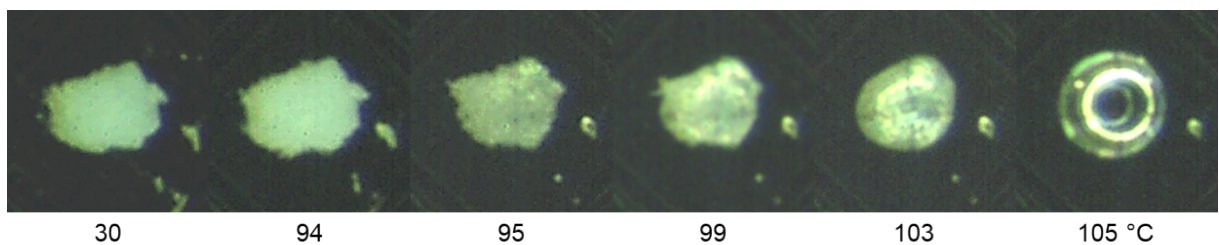


Fig. S7 Thermomicroscopy images in polarized reflected light of β polymorph, prepared by crystallization of PBZ from solution in EtOH at RT

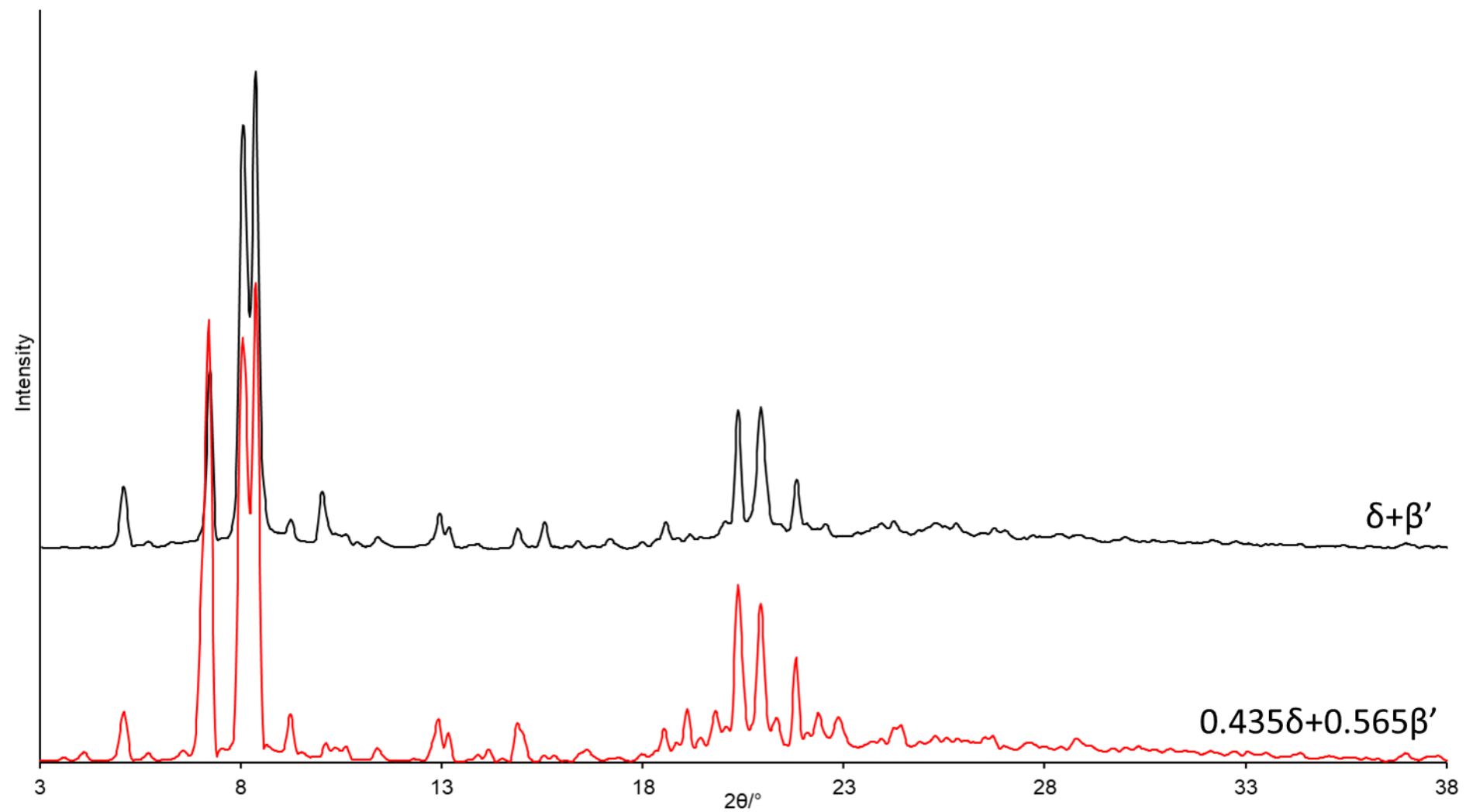


Fig S8. Comparison of powder X-ray diffractograms of $\delta+\beta'$ form prepared by drying of $\text{PBZ}\cdot\text{CH}_3\text{CN}$ solvate at RT and a sum of diffractogram of δ and β' forms in a ratio of 0.435:0.565. Diffractograms are corrected using standard silicon powder SRM 640d, and background was subtracted.

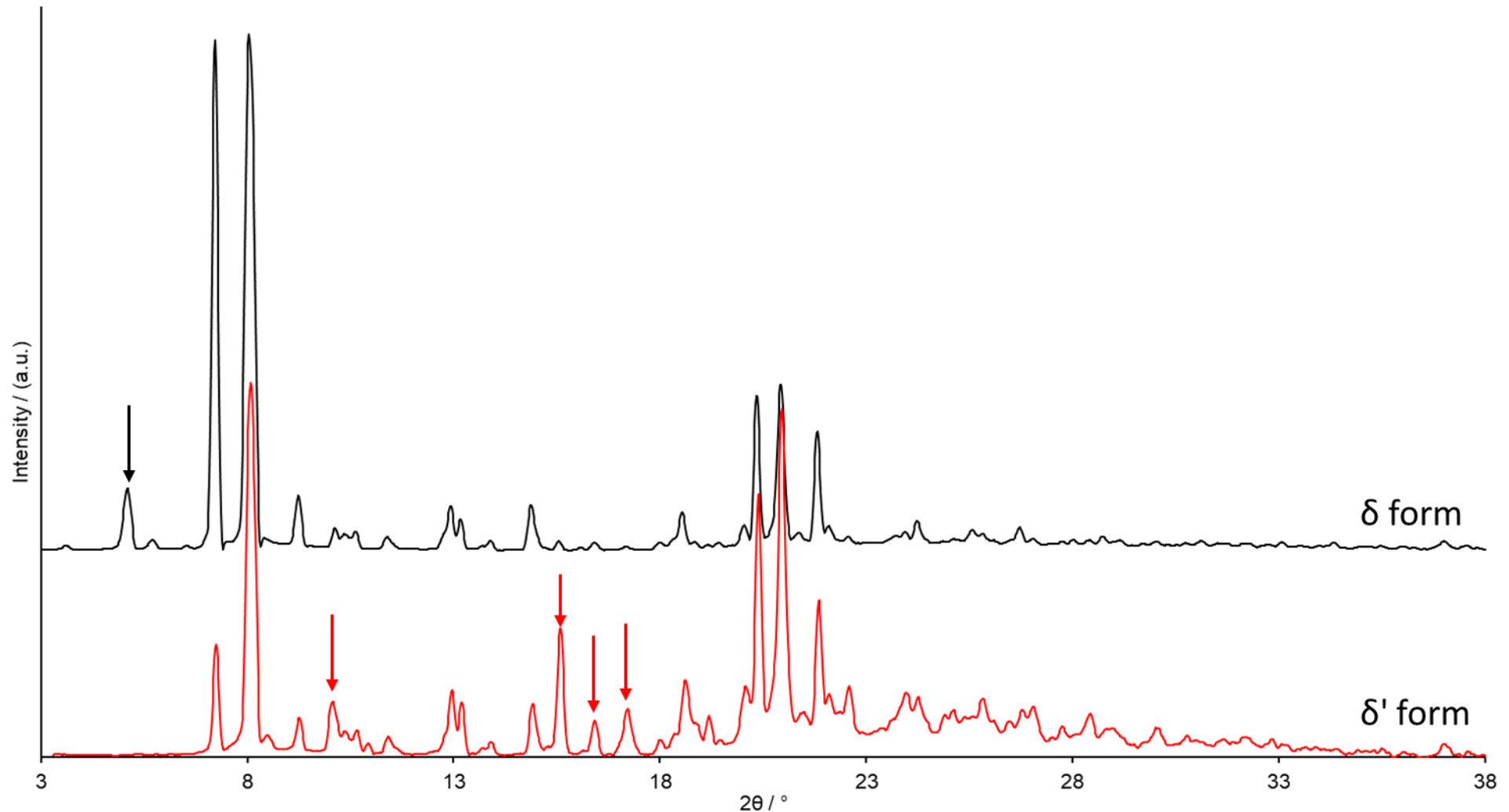


Fig. S9 Comparison of powder X-ray diffractograms of δ (commercial form) form and δ' prepared by heating the $\delta+\beta'$ form to 92 °C and cooling to RT in air. Diffractograms are corrected using standard silicon powder SRM 640d, and background was subtracted. Arrows indicate peaks with significant difference in position or relative intensity.

Table S1. Main PXRD peaks of PBZ polymorphs and guest-free forms

Forms of PBZ	Main PXRD peaks, 2θ (°) ^a	Unique X-ray diffraction peaks 2θ (deg) Literature data
α ^b	6.59; 8.48, 8.93, 12.48, 13.28, 15.78, 19.15, 19.57 20.15, 21.21, 21.44, 21.74, 23.56, 23.95, 24.52, 25.81	8.55° [1], 6.7°, 9.0°, 13.3° [2]
β ^c	4.09, 7.06, 8.38, 12.85, 15.06, 15.82, 16.63, 17.44, 19.12, 19.83, 20.20, 20.45, 21.13, 22.44, 22.88	7.1°, 8.4°, 16.5° [2]
β ^d	7.03, 8.36, 12.85, 15.08, 15.80, 16.61, 17.45, 19.08, 20.17, 20.46, 21.13, 22.44	
β ^e	7.08, 8.40, 12.87, 15.11, 15.89, 16.66, 19.14, 20.52, 21.05, 22.46	
β'	4.10, 7.07, 8.37, 12.85, 14.17, 15.03, 15.80, 16.61, 19.11, 19.81, 20.45, 21.01, 21.31, 22.37, 22.43, 22.87	-
δ ^f	5.09, 7.22, 8.05, 9.24, 12.93, 13.16, 14.87, 18.54, 20.35, 20.93, 21.81	8.05° [1], 20.92° [3]
δ ^g	5.08, 7.22, 8.07, 8.53, 9.24, 12.94, 13.18, 14.89, 18.60	
δ+β'	5.09, 7.23, 8.06, 8.37, 9.24, 10.03, 12.95, 13.18, 14.89, 15.56, 18.57, 20.37, 20.94, 21.83, 22.55	-
δ'	7.24, 8.08, 9.26, 10.06, 12.96, 13.18, 14.91, 15.59, 16.42 ^g , 17.22 ^g , 18.62, 20.39, 20.96, 21.85, 22.58	-

Notes: ^a Corrected using standard silicon powder SRM 640d; ^b prepared in PBZ·0.44*c*-C₆H₁₂+*n*-C₆H₁₄ (vap) system; ^c prepared by cooling PBZ melt in air; ^d prepared by cooling PBZ melt in argon flow; ^e prepared from PBZ solution in ethanol, ^f commercial form, ^g prepared in PBZ·0.44*c*-C₆H₁₂+EtOH (vap) system.

References

1. S. Datta and D. J. W. Grant, Cryst. Res. Technol., 2005, 40, 233–242.
2. N. Kaneniwa, J. Ichikawa, T. Matsumoto, Chem. Pharm. Bull., 1988, 36, 1063–1073.
3. Liang, S. Wang, Y. Qu, Journal of Chemical & Engineering Data. 2017, 62, 864–871.

Indexation of PBZ polymorphs

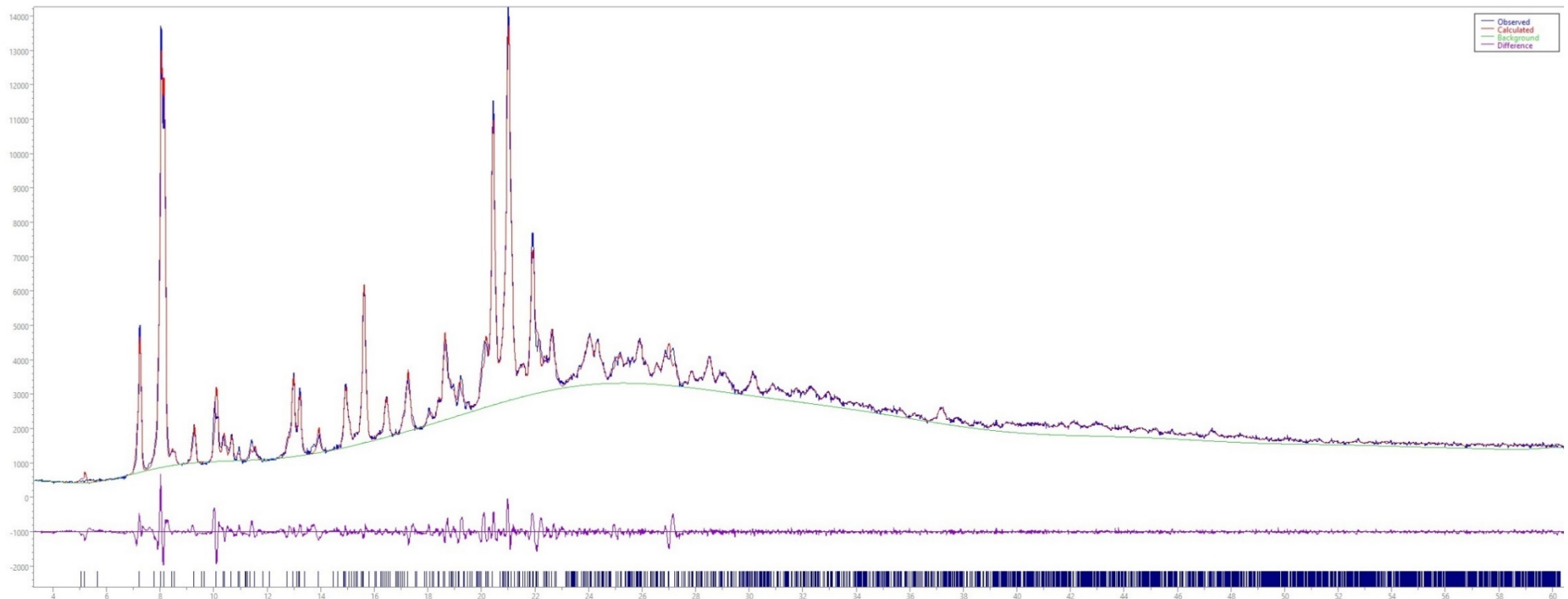


Fig. S10 Indexing results for XRPD diffractogram of δ' form with experimental pattern (blue), best fit (red) and differential curve (purple). Cell parameters: $a = 18.32809 \text{ \AA}$, $b = 34.13262 \text{ \AA}$, $c = 11.51791 \text{ \AA}$, $\alpha = 90.000^\circ$, $\beta = 106.986^\circ$, $\gamma = 90.000^\circ$, $V = 6891.11 \text{ \AA}^3$, $R_{\text{wp}} = 3.97\%$.

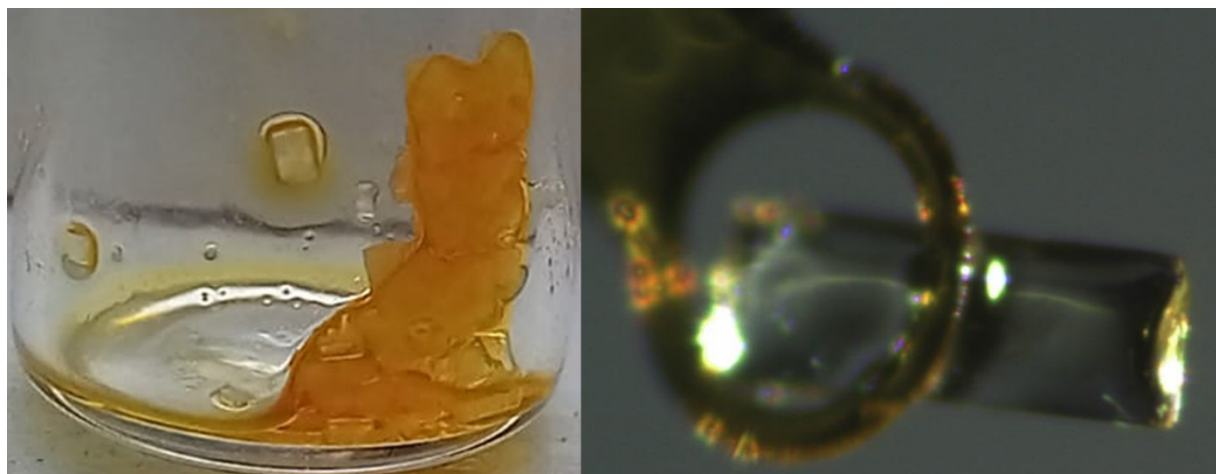
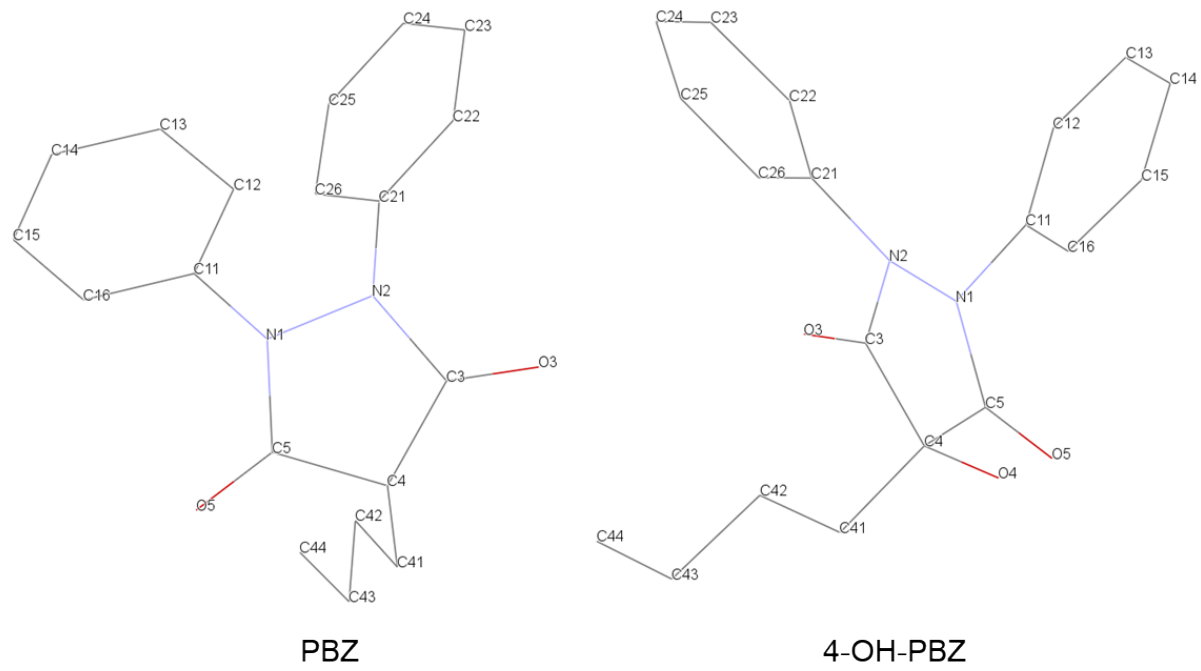


Fig. S11 Images of the 4-OH-PBZ crystals.

Table S2 Torsion and dihedral angles of phenylbutazone in crystals of PBZ·MeCN solvate and of its oxidized form 4-OH-PBZ.



Sample	τ_1 ($^{\circ}$)	τ_2 ($^{\circ}$)	ϕ ($^{\circ}$)
PBZ·MeCN	N2–N1–C11–C12 18.0(6)	N1–N2–C21–C26 40.9(6)	C22–C21–C26; C12–C11–C16 88.8(3)
4-HO-PBZ	N2–N1–C11–C12 19.95(15)	N1–N2–C21–C26 34.92(15)	C22–C21–C26; C12–C11–C16 85.10(6)

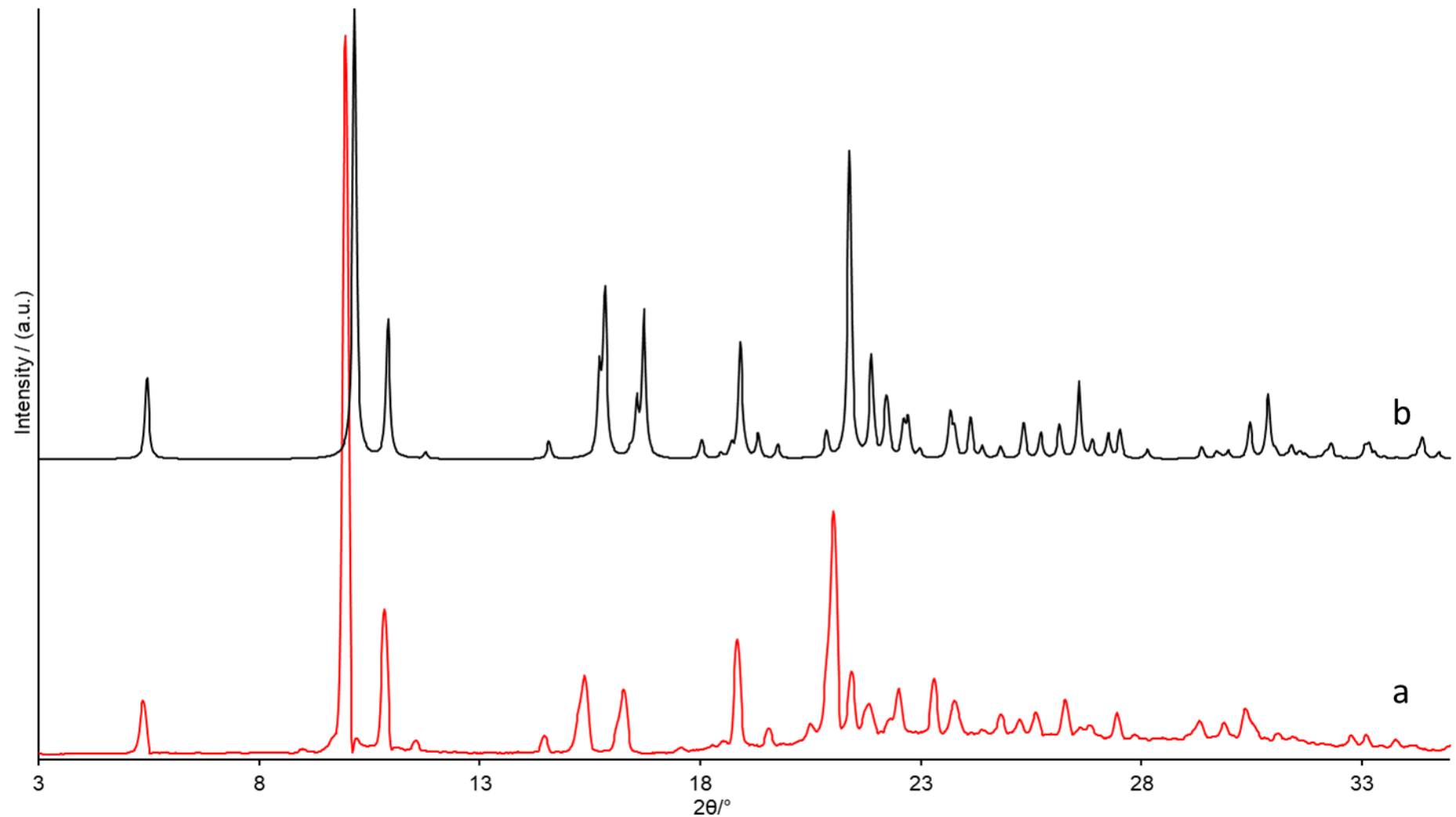


Fig. S12 Powder X-ray diffractograms of 4-OH-PBZ: (a) experimental at RT, (b) simulated from the single crystal X-ray diffraction data obtained at 100 K.

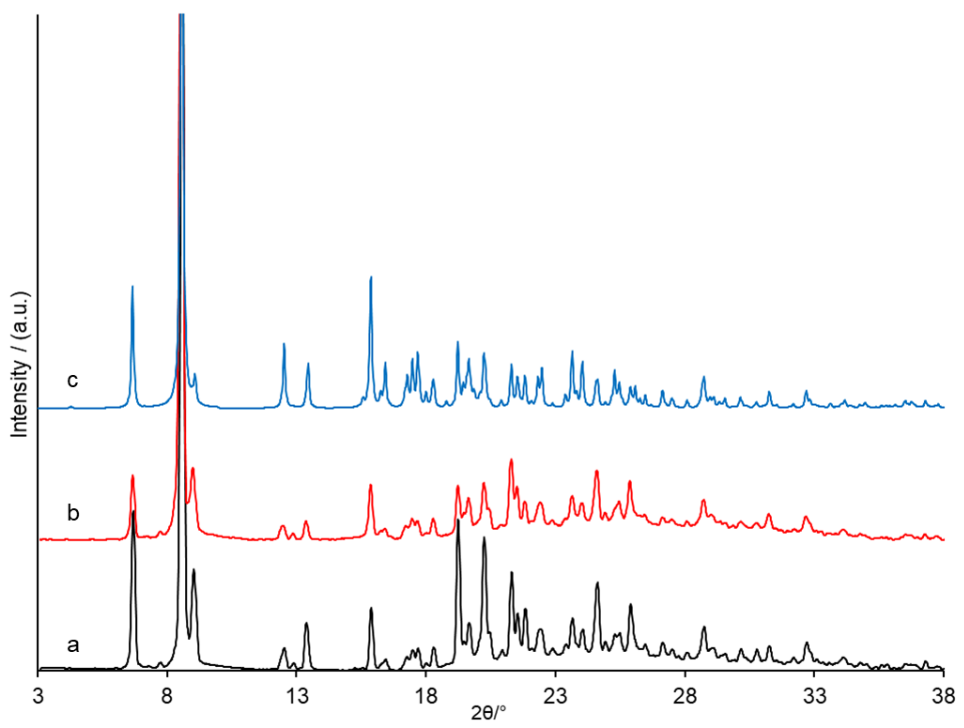


Fig. S13 Powder X-ray diffractograms of α polymorph of phenylbutazone: (a) prepared by dissolution of PBZ·0.20CCl₄ solvate in ethanol and subsequent crystallization at RT, (b) prepared by sequential saturation of PBZ with *c*-hexane and *n*-hexane vapors, (c) powder diffractogram simulated from literature single crystal X-ray diffraction data [T. P. Singh and M. Vijayan, J. Chem. Soc. Perkin Trans. 1977, 2, 693–699]. Experimental diffractograms are corrected using standard silicon powder SRM 640d, and background was subtracted.

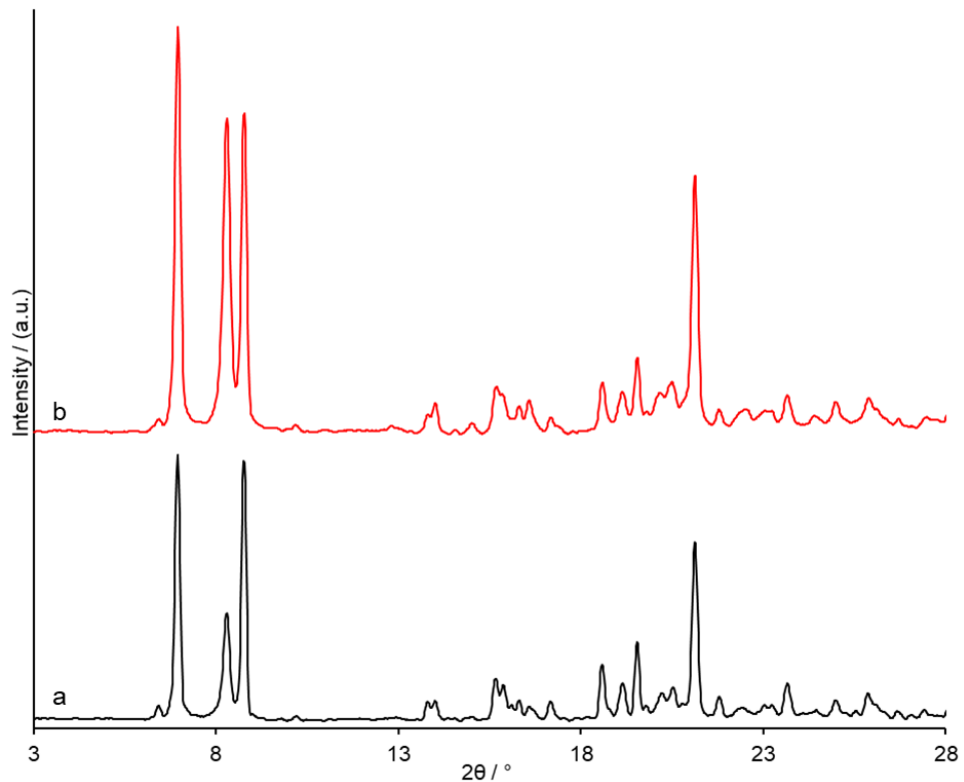


Fig. S14 Powder X-ray diffraction patterns of (a) PBZ solvate with carbon tetrachloride PBZ·0.20CCl₄ and (b) product of its saturation with *n*-hexane vapors. Diffractograms are corrected using standard silicon powder SRM 640d, and background was subtracted.

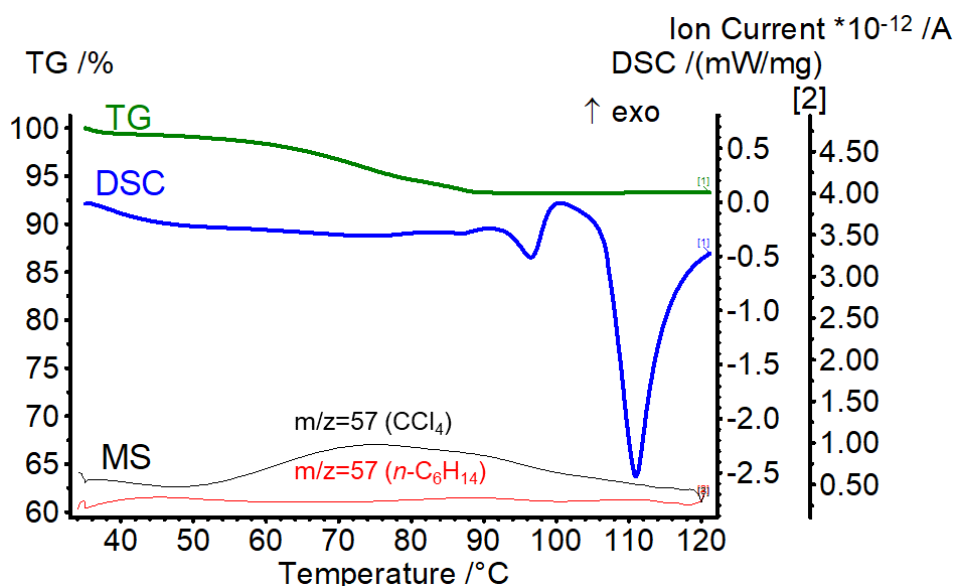


Fig. S15 TG/DSC/MS data for the product of PBZ·0.20CCl₄ saturation with n-hexane vapor.

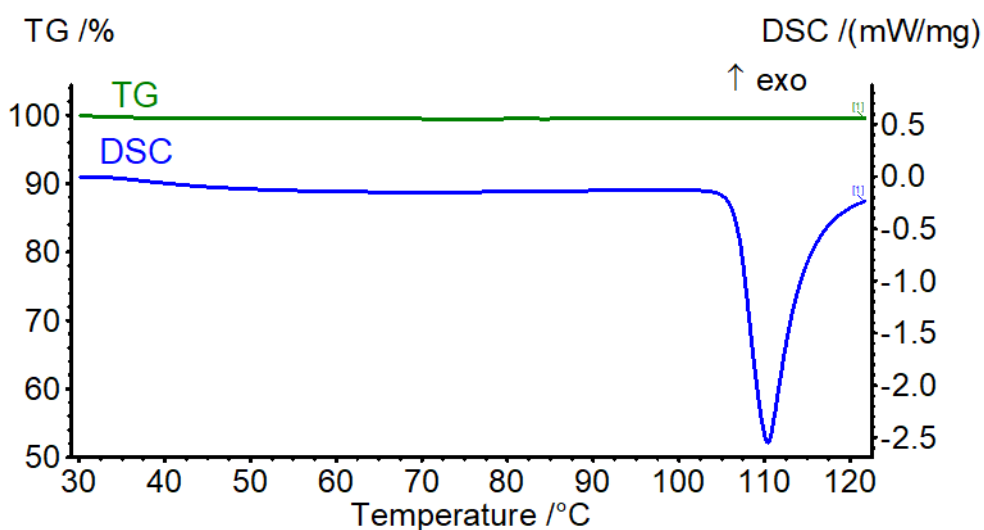


Fig. S16 TG/DSC data for δ form prepared by guest repulsion from PBZ·0.44c-C₆H₁₂ with EtOH vapor (onset point $T_m=106.6\text{ }^{\circ}\text{C}$, fusion enthalpy $\Delta H=23.4\text{ kJ mol}^{-1}$).

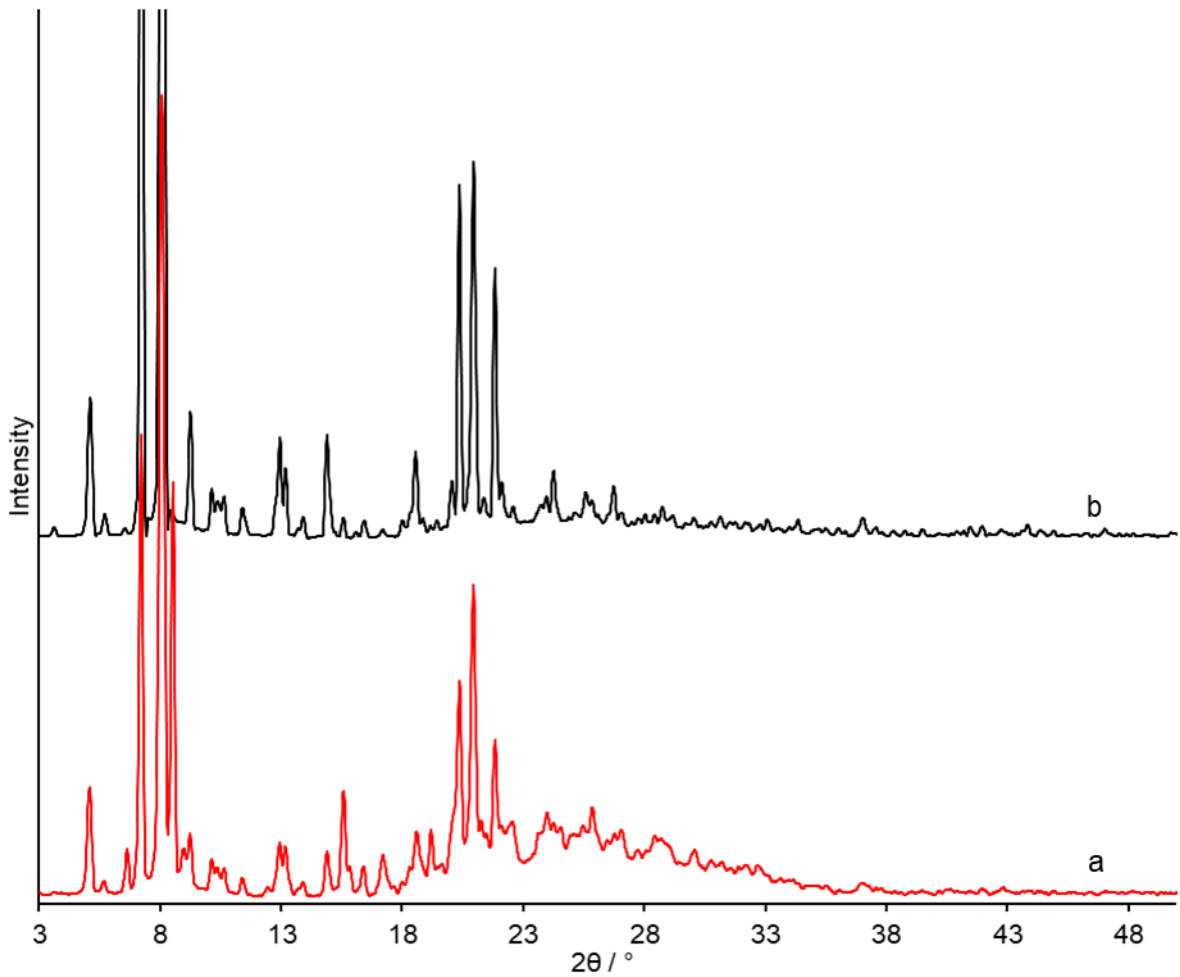


Fig. S17 Comparison of PXRD patterns of δ form: (a) prepared by guest repulsion from PBZ·0.44*c*-C₆H₁₂) with EtOH vapor, (b) commercial δ form of phenylbutazone. Diffractograms are corrected using standard silicon powder SRM 640d, and background was subtracted.

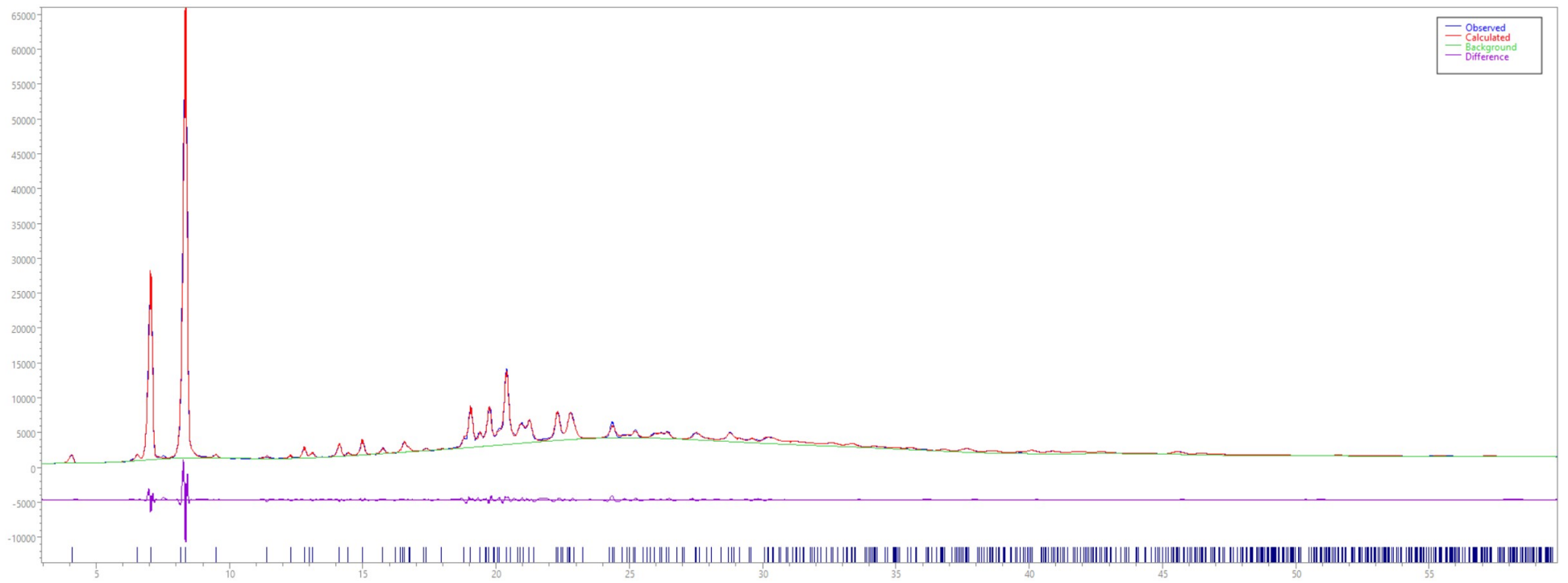


Fig. S18 Indexing results for XRPD diffractogram of β' polymorph with experimental pattern (blue), best fit (red) and differential curve (purple). Cell parameters: $a = 21.97666 \text{ \AA}$, $b = 5.82468 \text{ \AA}$, $c = 13.73231 \text{ \AA}$, $\alpha = 90.000^\circ$, $\beta = 100.735^\circ$, $\gamma = 90.000^\circ$, $V = 1727.07 \text{ \AA}^3$, $R_{wp} = 2.67\%$.

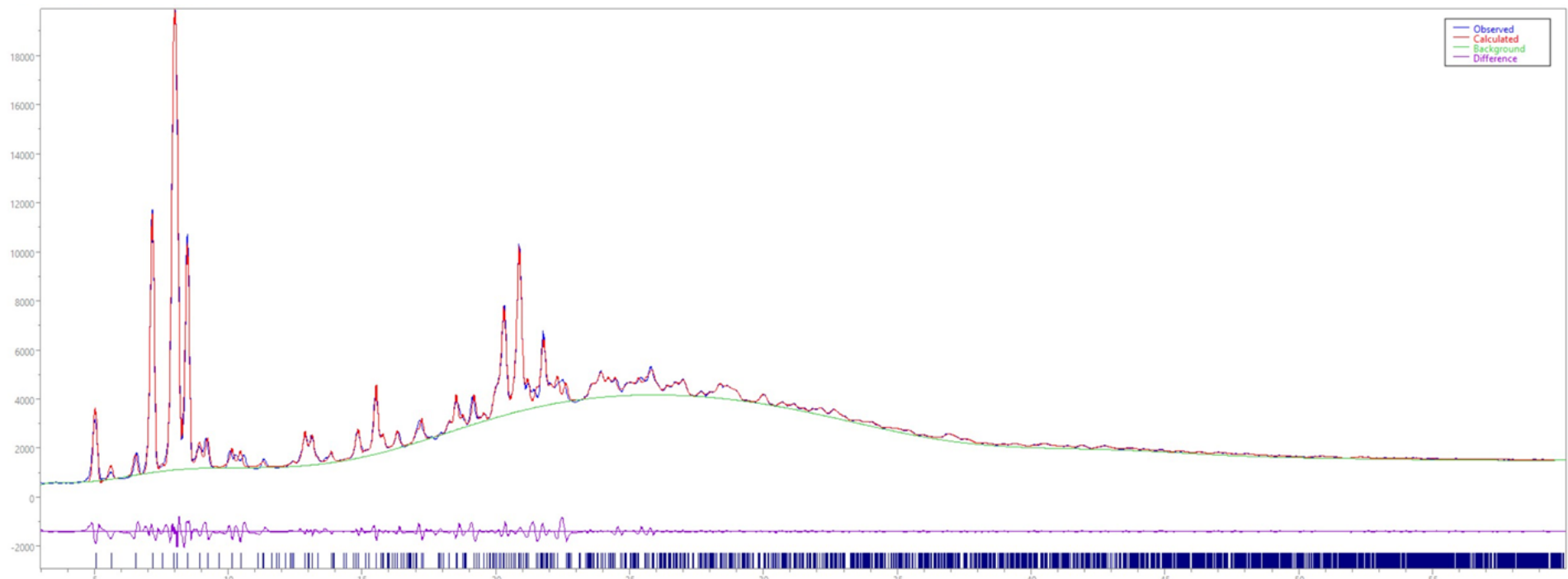


Fig. S19 Indexing results for XRPD diffractogram of δ polymorph, prepared in ‘PBZ·0.44c-C₆H₁₂ + EtOH (vap.)’ system with experimental pattern (blue), best fit (red) and differential curve (purple). Cell parameters: $a = 17.50336 \text{ \AA}$, $b = 16.19190 \text{ \AA}$, $c = 13.88016 \text{ \AA}$, $\alpha = 103.872^\circ$, $\beta = 91.430^\circ$, $\gamma = 95.448^\circ$, $V = 3797.18 \text{ \AA}^3$, $R_{wp} = 3.090\%$

Table S3. Lists of PXRD peaks for phenylbutazone polymorphs, guest-free forms and solvates. Peak positions are corrected by determination of diffractogram of the same sample with an additive of standard silicon powder SRM 640d.

α polymorph prepared in PBZ·0.44 <i>c</i> -C ₆ H ₁₂ + <i>n</i> -C ₆ H ₁₄ (vap) system				β polymorph prepared by cooling PBZ melt in air			
Peak No.	Peak position, 2θ , °	Peak intensity	Background	Peak No.	Peak position, 2θ , °	Peak intensity	Background
1	6.59	6019	49	1	4.09	471	104
2	8.48	34673	117	2	7.06	7827	175
3	8.93	3782	169	3	8.38	19620	1
4	12.42	933	49	4	12.85	462	60
5	13.28	1886	375	5	15.06	738	125
6	15.78	2522	530	6	15.82	4072	104
7	18.20	807	482	7	16.63	5365	107
8	19.15	5692	489	8	17.44	1566	649
9	19.57	1752	571	9	19.12	2743	1063
10	20.15	5027	660	10	19.83	2315	1136
11	21.21	3689	628	11	20.20	4511	1121
12	21.44	2112	528	12	20.45	4199	816
13	21.74	2293	600	13	21.13	3193	444
14	22.32	1501	678	14	22.44	5308	515
15	23.56	1914	563	15	22.88	1949	665
16	23.95	1513	147	16	24.43	3521	748
17	24.52	3293	415	17	24.98	1454	807
18	25.81	2481	415	18	25.32	1324	910
19	28.64	1607	415	19	26.19	1871	361
				20	27.62	1494	568
				21	28.82	920	504
				22	30.38	1282	523
β polymorph prepared by cooling PBZ melt in argon flow				β polymorph prepared from PBZ solution in ethanol			
Peak No.	Peak position, 2θ , °	Peak intensity	Background	Peak No.	Peak position, 2θ , °	Peak intensity	Background
1	7.03	4218	142	1	7.08	12219	384
2	8.36	10836	161	2	8.40	39334	525
3	12.85	237	0	3	12.87	453	553
4	15.08	303	239	4	13.17	385	812
5	15.80	1060	441	5	14.18	623	1036
6	16.61	1489	514	6	15.11	896	1131
7	17.45	341	546	7	15.89	317	939
8	17.92	123	490	8	16.66	692	860
9	19.08	1016	383	9	19.14	1944	780
10	19.83	795	301	10	19.46	1597	780
11	20.17	1536	301	11	19.84	2903	780
12	20.46	1836	301	12	20.52	3526	780
13	21.13	1279	301	13	21.05	2387	780
14	22.44	1432	301	14	22.46	1781	780
15	24.42	1097	301	15	22.94	2475	780
16	26.18	776	301	16	24.51	1441	780
17	27.60	606	301				

β' form				δ polymorph (commercial)			
Peak No.	Peak position, $2\theta, {}^\circ$	Peak intensity	Background	Peak No.	Peak position, $2\theta, {}^\circ$	Peak intensity	Background
1	4.10	702	191	1	5.09	5268	30
2	7.07	16220	293	2	7.22	44054	494
3	8.37	39026	625	3	8.05	44439	593
4	12.85	889	1079	4	9.24	4699	227
5	14.17	1026	1269	5	10.12	1811	203
6	15.03	1298	1101	6	10.62	1500	136
7	15.80	474	901	7	12.93	3759	20
8	16.61	935	550	8	13.16	2577	35
9	19.11	4049	610	9	14.87	3750	318
10	19.81	3870	671	10	18.54	3196	348
11	20.45	7555	729	11	20.04	2082	433
12	21.01	2334	729	12	20.35	13359	586
13	21.31	2542	729	13	20.93	14292	771
14	22.37	3391	729	14	21.81	10215	787
15	22.87	3287	729	15	22.09	2025	594
16	24.43	2256	729	16	24.24	2471	285
				17	26.72	1900	366
δ polymorph prepared in PBZ·0.44 <i>c</i> -C ₆ H ₁₂ +EtOH (vap) system				δ' form			
Peak No.	Peak position, $2\theta, {}^\circ$	Peak intensity	Background	Peak No.	Peak position, $2\theta, {}^\circ$	Peak intensity	Background
1	5.08	2515	49	1	7.24	2391	57
2	5.68	261	105	2	8.08	8062	118
3	6.64	1040	282	3	9.26	796	111
4	7.22	10878	361	4	10.06	1154	51
5	8.07	19010	301	5	11.42	400	33
6	8.53	9800	217	6	12.96	1268	31
7	8.98	1062	168	7	13.18	1147	77
8	9.24	1424	76	8	14.91	1105	207
9	10.13	823	31	9	15.59	2758	205
10	10.64	595	41	10	16.42	748	167
11	11.41	352	46	11	17.22	965	424
12	12.94	1197	7	12	18.37	455	540
13	13.18	1046	447	13	18.62	1612	692
14	14.89	955	404	14	19.19	844	729
15	15.58	2433	683	15	20.08	1484	691
16	15.82	617	915	16	20.39	5686	644
17	16.40	635	1031	17	20.96	7501	531
18	17.20	835	1142	18	21.48	925	924
19	18.60	1461	1006	19	21.85	3365	907
20	19.20	1497	1468	20	22.10	1311	784
				21	22.58	1496	693
				22	23.97	1352	222
				23	24.26	1261	231
				24	25.83	1215	474

$\delta+\beta'$ form				PBZ·0.15C ₆ H ₆			
Peak No.	Peak position, $2\theta, {}^\circ$	Peak intensity	Background	Peak No.	Peak position, $2\theta, {}^\circ$	Peak intensity	Background
1	5.09	3552	513	1	6.49	1638	606
2	7.23	10367	632	2	7.14	32745	1166
3	8.06	24627	631	3	8.34	4782	1208
4	8.37	27671	485	4	9.15	6040	581
5	9.24	1650	219	5	15.89	2798	197
6	10.03	3264	40	6	18.68	2749	819
7	11.41	623	15	7	19.46	6124	1380
8	12.95	2017	9	8	20.13	3428	1502
9	13.18	1174	184	9	21.40	6313	2151
10	14.89	1142	1459	10	22.28	2312	1890
11	15.56	1474	1628	11	23.35	2560	747
12	18.57	1479	742	12	24.87	1694	785
13	20.37	7999	571	13	25.43	1549	793
14	20.94	8197	830	14	27.74	1656	317
15	21.83	3970	569	15	30.68	1270	857
16	22.55	1372	569				
17	24.25	1543	569				
PBZ·0.35CHCl ₃				PBZ·0.44c-C ₆ H ₁₂			
Peak No.	Peak position, $2\theta, {}^\circ$	Peak intensity	Background	Peak No.	Peak position, $2\theta, {}^\circ$	Peak intensity	Background
1	7.36	37989	1062	1	6.95	132688	2710
2	8.35	2825	1007	2	8.36	23918	2508
3	9.74	7933	34	3	8.84	32742	2201
4	12.76	927	67	4	13.90	4740	2900
5	13.38	473	68	5	15.93	13136	3286
6	14.71	1835	516	6	17.19	5997	4099
7	16.05	2994	537	7	18.59	11611	5421
8	16.95	942	751	8	19.16	9962	6443
9	19.52	3075	1418	9	19.55	25497	8056
10	19.71	2241	1504	10	20.38	13117	7623
11	20.73	3898	1404	11	20.99	32414	6016
12	22.11	36067	568	12	21.67	9393	5796
13	22.47	4100	370	13	22.38	8903	5456
14	23.05	8002	716	14	23.11	9659	5670
15	26.68	2601	716	15	23.55	11887	4870
16	28.99	2010	716	16	24.84	8773	4870
				17	26.14	9281	4870

PBZ·0.2CCl ₄			
Peak No.	Peak position, $2\theta, {}^\circ$	Peak intensity	Background
1	6.50	227	58
2	7.02	4177	88
3	8.37	1741	100
4	8.84	4228	95
5	13.87	281	0
6	14.08	281	17
7	15.73	622	18
8	15.94	529	162
9	16.38	293	266
10	16.66	198	330
11	17.23	327	371
12	18.65	1029	459
13	19.21	803	517
14	19.61	1538	559
15	20.29	747	609
16	20.59	883	605
17	21.19	3371	594
18	21.86	831	580
19	23.72	1130	475
20	25.05	858	455
21	25.93	939	496